(Received 17 February 2025, Accepted 8 July 2025, Scheduled 8 August 2025)

Transfer Matrix Method for General Bianisotropic Layers

Morgan A. Blankenship, Edgar Bustamante, and Raymond C. Rumpf*

Department of Electrical and Computer Engineering, University of Texas at El Paso, El Paso, TX 79968, USA

ABSTRACT: The transfer matrix method (TMM) with scattering matrices has been a valuable tool, facilitating the characterization of multilayer devices in a very fast, stable, and memory-efficient manner. This paper presents a generalization of TMM with improved scattering matrices capable of simulating devices with full nine-element material tensors for the layers and any combination of signs for the real and imaginary parts of the isotropic external regions. The formulation of the bianisotropic transfer matrix method (BTMM) algorithm is covered in detail, and notes on implementation are provided. Example devices found in literature were used to benchmark the accuracy of the algorithm. The simulation of the bianisotropic device was corroborated with a finite-difference frequency-domain (FDFD) algorithm and a finite-element method (FEM).

1. INTRODUCTION

The classic TMM algorithm [1] is a semi-analytical frequency-domain method which analyzes wave propagation through stratified homogeneous media [2, 3]. Most commonly, TMM has been used to calculate the overall reflection and transmission from thin film optical filters [2], although it has also been used in dispersion analysis [4–6], slab waveguide analysis [7], construction of band diagrams [8], transmission line analysis using circuit-wave equivalence [9], and analyzing effective properties via parameter retrieval [10, 11]. Transfer matrix method serves as a very fast method for preliminary results before turning to more sophisticated methods such as rigorous coupled-wave analysis [12, 13], plane-wave expansion method [14], or finite-difference frequency-domain [15, 16].

The literature contains some work on extending TMM to handle bianisotropy. However, each has only considered limited bianisotropy [17–20], assumed simplified tensor symmetry [17, 18, 20], or were unstable [21, 22]. Yin et al. [21] and Mackay and Lakhtakia [22] derived the same eigenvalue problem presented here, but applied it to more constrained configurations. The former analyzed radiation characteristics of a dipole antenna on grounded bianisotropic multilayers [21] and did not consider total reflection and transmission. The latter utilized transfer matrices, known to be unstable for thick layers or media with extreme properties. No TMM formulation surveyed was able to handle full nine-element tensors, regardless of symmetry, and the effect of complex-valued external regions in a stable manner.

Outside of TMM, full bianisotropy can be simulated using finite-element [23, 24] or finite-difference [25] based methods. While these formulations are more flexible in terms of allowed geometries, they are significantly more difficult to implement in practice and require substantially higher computational resources than TMM. This makes fine resolution parameter sweeps over wavelength, incidence angles, and/or polarization for relatively simple geometries more time and memory consuming than necessary. The comparison of the time and memory required among the present BTMM algorithm, a bianisotropic finite-element method (BFEM), and a bianisotropic finite-difference frequency-domain method (BFDFD) is discussed in the benchmarking section. Additionally, demonstrations of these alternative methods are typically restricted to skew- or Hermitian-symmetric bianisotropy, purely real or imaginary bianisotropic coupling, and/or sparse bianisotropic tensors. To the authors' knowledge, the present work is the first bianisotropic-capable method that explicitly showcases a full tensor simulation without instability or nonphysical results.

The following algorithm is introduced to efficiently and stably simulate stratified bianisotropic media, like the one illustrated in Figure 1. It supports independent and full bianisotropic tensors without assumptions on symmetry, which is essential for validating any possible effective parameters from homogenized metamaterials [26–28]. It accommodates any combination of signs for the external regions, enabling the simulation of complex or metamaterial-inspired surrounding media. Its computational efficiency is practical for extensive parameter sweeps, accelerating the design and exploration of novel bianisotropic metamaterials. The only known limitation of the algorithm occurs when the system becomes singular, or the real part of the reflection-side refractive index is zero $\mathrm{Re}[n_{\mathrm{ref}}] = 0$, and one or more layers are considered.

2. FORMULATION

The BTMM algorithm is derived from frequency-domain Maxwell's curl equations in bianisotropic media, given by

$$\nabla \times \vec{E} = -jk_0 \left([\mu_{\mathrm{r}}] \vec{H} + [\zeta_{\mathrm{r}}] \vec{E} \right), \tag{1}$$

$$\nabla \times \vec{H} = jk_0 \left([\varepsilon_{\mathrm{r}}] \vec{E} + [\xi_{\mathrm{r}}] \vec{H} \right), \tag{2}$$

* Corresponding author: Raymond C. Rumpf (rcrumpf@utep.edu).

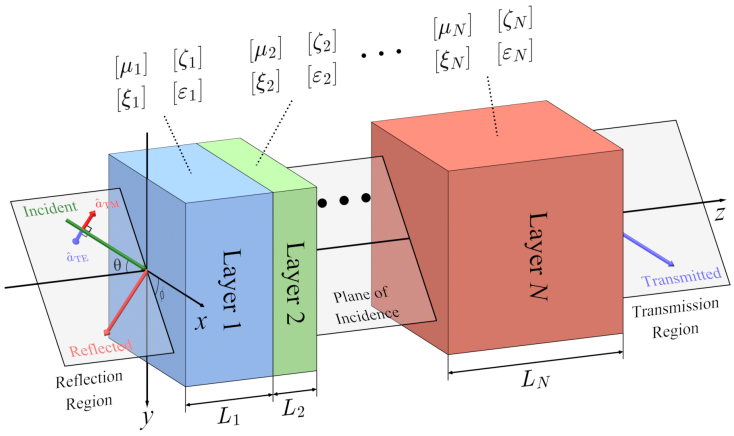

FIGURE 1. Geometry of the BTMM problem where an incident wave on a stack of bianisotropic layers can reflect, transmit, and/or be absorbed.

where $\vec{E}$ is the electric field intensity; $\vec{\tilde{H}} = \eta_0 \vec{H}$ is the normalized magnetic field intensity; $k_0 = 2\pi/\lambda_0$ is the free-space wave number; and $j^2 = -1$. The complex 3×3 tensor quantities $[\mu_\mathrm{r}]$, $[\varepsilon_\mathrm{r}]$, $[\zeta_\mathrm{r}]$, and $[\xi_\mathrm{r}]$ are the relative permeability, permittivity, magneto-electric and electro-magnetic coupling tensors [29], respectively. These equations and material properties assume the negative sign convention where a wave propagating in the $+z$ direction is expressed as $\exp(-jk_0nz)$. The divergence equations are not required in this case since the following BTMM algorithm only utilizes the transverse components, i.e., x and y, of the electromagnetic wave. If the longitudinal components of the electromagnetic wave are desired, they must be calculated such that the divergence equations are satisfied.

2.1. Layer Eigenvalue Problem

The BTMM algorithm assumes that the device is homogeneous and infinite in two dimensions, typically the x and y directions. For this reason, the device along these directions can only contribute to phase accumulation. The partial derivatives with respect to x and y in Eqs. (1) and (2) are replaced analytically by $-j\tilde{k}_x$ and $-j\tilde{k}_y$, respectively. The normalized wavevector is defined as

$$\vec{\tilde{k}} = \frac{\vec{k}}{k_0} = \underbrace{+\sqrt{\mu_{\mathrm{r,ref}}\varepsilon_{\mathrm{r,ref}}}}_{n_\mathrm{ref}} \begin{bmatrix} \sin\theta\cos\phi \\ \sin\theta\sin\phi \\ \cos\theta \end{bmatrix}, \tag{3}$$

with the elevation θ and azimuthal ϕ angles of incidence defined in Figure 1. After applying these conditions, Maxwell's curl equations can be combined to arrive at the following differential equation used to calculate the electromagnetic modes within a bianisotropic layer,

$$\underbrace{\frac{d}{d\tilde{z}}\begin{bmatrix} E_x \\ E_y \\ \tilde{H}_x \\ \tilde{H}_y \end{bmatrix}}_{\psi} = \frac{-j}{\Omega_0} \underbrace{\begin{bmatrix} \Omega_{11} & \Omega_{12} & \Omega_{13} & \Omega_{14} \\ \Omega_{21} & \Omega_{22} & \Omega_{23} & \Omega_{24} \\ \Omega_{31} & \Omega_{32} & \Omega_{33} & \Omega_{34} \\ \Omega_{41} & \Omega_{42} & \Omega_{43} & \Omega_{44} \end{bmatrix}}_{\mathbf{\Omega}} \underbrace{\begin{bmatrix} E_x \\ E_y \\ \tilde{H}_x \\ \tilde{H}_y \end{bmatrix}}_{\psi}, \tag{4}$$

where $\tilde{z} = k_0 z$. The $\mathbf{\Omega}$ matrix represents a matrix operator that incorporates the complex interactions between an electromagnetic wave and bianisotropic materials such that Maxwell's curl equations are satisfied. The $\mathbf{\Omega}$ matrix components themselves do not possess any significant physical meaning. Expressions for each element are easily shown to be

$$\begin{aligned}
\Omega_{11} &= \zeta_{yx}\Omega_0 + \varepsilon_{zx}\left\{\mu_{yz}\zeta_{zz} - \mu_{zz}\left(\tilde{k}_x + \zeta_{yz}\right)\right\} \\
&\quad + \left(\zeta_{zx} + \tilde{k}_y\right)\left\{\xi_{zz}\left(\tilde{k}_x + \zeta_{yz}\right) - \mu_{yz}\varepsilon_{zz}\right\}, \quad (5) \\
\Omega_{12} &= \zeta_{yy}\Omega_0 + \varepsilon_{zy}\left\{\mu_{yz}\zeta_{zz} - \mu_{zz}\left(\tilde{k}_x + \zeta_{yz}\right)\right\} \\
&\quad + \left(\zeta_{zy} - \tilde{k}_x\right)\left\{\xi_{zz}\left(\tilde{k}_x + \zeta_{yz}\right) - \mu_{yz}\varepsilon_{zz}\right\}, \quad (6) \\
\Omega_{13} &= \mu_{yx}\Omega_0 + \mu_{zx}\left\{\xi_{zz}\left(\tilde{k}_x + \zeta_{yz}\right) - \mu_{yz}\varepsilon_{zz}\right\} \\
&\quad + \left(\xi_{zx} - \tilde{k}_y\right)\left\{\mu_{yz}\zeta_{zz} - \mu_{zz}\left(\tilde{k}_x + \zeta_{yz}\right)\right\}, \quad (7) \\
\Omega_{14} &= \mu_{yy}\Omega_0 + \mu_{zy}\left\{\xi_{zz}\left(\tilde{k}_x + \zeta_{yz}\right) - \mu_{yz}\varepsilon_{zz}\right\} \\
&\quad + \left(\xi_{zy} + \tilde{k}_x\right)\left\{\mu_{yz}\zeta_{zz} - \mu_{zz}\left(\tilde{k}_x + \zeta_{yz}\right)\right\}, \quad (8) \\
\Omega_{21} &= \varepsilon_{zx}\left\{\mu_{xz}\zeta_{zz} - \mu_{zz}\left(\tilde{k}_y - \zeta_{xz}\right)\right\} - \zeta_{xx}\Omega_0 \\
&\quad + \left(\zeta_{zx} + \tilde{k}_y\right)\left\{\xi_{zz}\left(\tilde{k}_y - \zeta_{xz}\right) - \mu_{xz}\varepsilon_{zz}\right\}, \quad (9) \\
\Omega_{22} &= \varepsilon_{zy}\left\{\mu_{xz}\zeta_{zz} - \mu_{zz}\left(\tilde{k}_y - \zeta_{xz}\right)\right\} - \zeta_{xy}\Omega_0 \\
&\quad + \left(\zeta_{zy} - \tilde{k}_x\right)\left\{\xi_{zz}\left(\tilde{k}_y - \zeta_{xz}\right) - \mu_{xz}\varepsilon_{zz}\right\}, \quad (10) \\
\Omega_{23} &= \mu_{zx}\left\{\xi_{zz}\left(\tilde{k}_y - \zeta_{xz}\right) - \mu_{xz}\varepsilon_{zz}\right\} - \mu_{xx}\Omega_0 \\
&\quad + \left(\xi_{zx} - \tilde{k}_y\right)\left\{\mu_{xz}\zeta_{zz} - \mu_{zz}\left(\tilde{k}_y - \zeta_{xz}\right)\right\}, \quad (11) \\
\Omega_{24} &= \mu_{zy}\left\{\xi_{zz}\left(\tilde{k}_y - \zeta_{xz}\right) - \mu_{xz}\varepsilon_{zz}\right\} - \mu_{xy}\Omega_0 \\
&\quad + \left(\xi_{zy} + \tilde{k}_x\right)\left\{\mu_{xz}\zeta_{zz} - \mu_{zz}\left(\tilde{k}_y - \zeta_{xz}\right)\right\}, \quad (12)
\end{aligned}$$

$$\Omega_{31} = \varepsilon_{zx}\left\{\varepsilon_{yz}\mu_{zz}+\zeta_{zz}\left(\tilde{k}_x-\xi_{yz}\right)\right\}-\varepsilon_{yx}\Omega_0 - \left(\zeta_{zx}+\tilde{k}_y\right)\left\{\varepsilon_{zz}\left(\tilde{k}_x-\xi_{yz}\right)+\varepsilon_{yz}\xi_{zz}\right\}, \quad (13)$$

$$\Omega_{32} = \varepsilon_{zy}\left\{\varepsilon_{yz}\mu_{zz}+\zeta_{zz}\left(\tilde{k}_x-\xi_{yz}\right)\right\}-\varepsilon_{yy}\Omega_0 - \left(\zeta_{zy}-\tilde{k}_x\right)\left\{\varepsilon_{zz}\left(\tilde{k}_x-\xi_{yz}\right)+\varepsilon_{yz}\xi_{zz}\right\}, \quad (14)$$

$$\Omega_{33} = -\mu_{zx}\left\{\varepsilon_{zz}\left(\tilde{k}_x-\xi_{yz}\right)+\varepsilon_{yz}\xi_{zz}\right\}-\xi_{yx}\Omega_0 + \left(\xi_{zx}-\tilde{k}_y\right)\left\{\varepsilon_{yz}\mu_{zz}+\zeta_{zz}\left(\tilde{k}_x-\xi_{yz}\right)\right\}, \quad (15)$$

$$\Omega_{34} = -\mu_{zy}\left\{\varepsilon_{zz}\left(\tilde{k}_x-\xi_{yz}\right)+\varepsilon_{yz}\xi_{zz}\right\}-\xi_{yy}\Omega_0 + \left(\xi_{zy}+\tilde{k}_x\right)\left\{\varepsilon_{yz}\mu_{zz}+\zeta_{zz}\left(\tilde{k}_x-\xi_{yz}\right)\right\}, \quad (16)$$

$$\Omega_{41} = \varepsilon_{xx}\Omega_0+\varepsilon_{zx}\left\{\zeta_{zz}\left(\tilde{k}_y+\xi_{xz}\right)-\varepsilon_{xz}\mu_{zz}\right\} + \left(\zeta_{zx}+\tilde{k}_y\right)\left\{\varepsilon_{xz}\xi_{zz}-\varepsilon_{zz}\left(\tilde{k}_y+\xi_{xz}\right)\right\}, \quad (17)$$

$$\Omega_{42} = \varepsilon_{xy}\Omega_0+\varepsilon_{zy}\left\{\zeta_{zz}\left(\tilde{k}_y+\xi_{xz}\right)-\varepsilon_{xz}\mu_{zz}\right\} + \left(\zeta_{zy}-\tilde{k}_x\right)\left\{\varepsilon_{xz}\xi_{zz}-\varepsilon_{zz}\left(\tilde{k}_y+\xi_{xz}\right)\right\}, \quad (18)$$

$$\Omega_{43} = \xi_{xx}\Omega_0+\mu_{zx}\left\{\varepsilon_{xz}\xi_{zz}-\varepsilon_{zz}\left(\tilde{k}_y+\xi_{xz}\right)\right\} + \left(\xi_{zx}-\tilde{k}_y\right)\left\{\zeta_{zz}\left(\tilde{k}_y+\xi_{xz}\right)-\varepsilon_{xz}\mu_{zz}\right\}, \quad (19)$$

$$\Omega_{44} = \xi_{xy}\Omega_0+\mu_{zy}\left\{\varepsilon_{xz}\xi_{zz}-\varepsilon_{zz}\left(\tilde{k}_y+\xi_{xz}\right)\right\} + \left(\xi_{zy}+\tilde{k}_x\right)\left\{\zeta_{zz}\left(\tilde{k}_y+\xi_{xz}\right)-\varepsilon_{xz}\mu_{zz}\right\}. \quad (20)$$

In these equations, $\Omega_0 = \mu_{zz}\varepsilon_{zz} - \xi_{zz}\zeta_{zz}$ which implies an unlikely but possible failure point when Ω_0 is zero. This term originates from an intermediate step when algebraically eliminating the E_z and $\tilde{H}_z$ dependence from Eqs. (1) and (2), resulting in the transverse component only system of Eq. (4). When Ω_0 vanishes, the wave vector in the direction of propagation $\tilde{k}_z$ also vanishes, and the $\mathbf{\Omega}$ matrix becomes singular. This is not only an unavoidable numerical limitation of the algorithm, but a physically observable one as well [30]. The general solution to Eq. (4) is calculated from the eigenvector $\mathbf{W}$ and eigenvalue $\mathbf{D}$ matrices of $\mathbf{\Omega}$ as

$$\boldsymbol{\psi}(\tilde{z}) = \underbrace{\begin{bmatrix} \mathbf{W}_E^+ & \mathbf{W}_E^- \\ \mathbf{W}_H^+ & \mathbf{W}_H^- \end{bmatrix}}_{\mathbf{W}} \underbrace{\begin{bmatrix} \text{expm}\left(\mathbf{D}^+\tilde{z}\right) & \mathbf{0} \\ \mathbf{0} & \text{expm}\left(\mathbf{D}^-\tilde{z}\right) \end{bmatrix}}_{\text{expm}(\mathbf{D}\tilde{z})} \begin{bmatrix} \mathbf{c}^+ \\ \mathbf{c}^- \end{bmatrix}, \quad (21)$$

where the $+$ or $-$ superscripts indicate forward or backward propagating modes, respectively; $\mathbf{0}$ is the zeros matrix; and $\text{expm}(\mathbf{D}\tilde{z})$ is the matrix exponential. A robust method to determine the direction of the eigenmodes is from the sign of their Poynting vector in the z direction. Without sorting these eigenmodes, the algorithm is unstable.

2.2. Scattering Matrices

The scattering matrices quantify the coupling between eigenmodes of adjacent layers. The method described in Ref. [4] was applied here to obtain the scattering matrix of the ith layer $\mathbf{S}^{(i)}$, defined as

$$\begin{bmatrix} \mathbf{c}_1^- \\ \mathbf{c}_2^+ \end{bmatrix} = \begin{bmatrix} \mathbf{S}_{11}^{(i)} & \mathbf{S}_{12}^{(i)} \\ \mathbf{S}_{21}^{(i)} & \mathbf{S}_{22}^{(i)} \end{bmatrix} \begin{bmatrix} \mathbf{c}_1^+ \\ \mathbf{c}_2^- \end{bmatrix}, \quad (22)$$

where the components are

$$\begin{bmatrix} \mathbf{S}_{11}^{(i)} & \mathbf{S}_{12}^{(i)} \\ \mathbf{S}_{21}^{(i)} & \mathbf{S}_{22}^{(i)} \end{bmatrix} = \begin{bmatrix} \mathbf{A}_{12}^{(i)} & -\mathbf{B}_{11}^{(i)} \\ \mathbf{A}_{22}^{(i)} & -\mathbf{B}_{21}^{(i)} \end{bmatrix}^{-1} \begin{bmatrix} -\mathbf{A}_{11}^{(i)} & \mathbf{B}_{12}^{(i)} \\ -\mathbf{A}_{21}^{(i)} & \mathbf{B}_{22}^{(i)} \end{bmatrix}, \quad (23)$$

$$\begin{bmatrix} \mathbf{A}_{11}^{(i)} & \mathbf{A}_{12}^{(i)} \\ \mathbf{A}_{21}^{(i)} & \mathbf{A}_{22}^{(i)} \end{bmatrix} = \begin{bmatrix} \mathbf{I} & \mathbf{0} \\ \mathbf{0} & \text{expm}\left(k_0\mathbf{D}_i^- L_i\right) \end{bmatrix} \mathbf{W}_i^{-1}\mathbf{W}_1, \quad (24)$$

$$\begin{bmatrix} \mathbf{B}_{11}^{(i)} & \mathbf{B}_{12}^{(i)} \\ \mathbf{B}_{21}^{(i)} & \mathbf{B}_{22}^{(i)} \end{bmatrix} = \begin{bmatrix} \text{expm}\left(-k_0\mathbf{D}_i^+ L_i\right) & \mathbf{0} \\ \mathbf{0} & \mathbf{I} \end{bmatrix} \mathbf{W}_i^{-1}\mathbf{W}_2. \quad (25)$$

The subscripts on $\mathbf{A}$ and $\mathbf{B}$ represent the 2×2 block matrix row-column indices, and $\mathbf{I}$ is the identity matrix. In the improved scattering matrix approach [4], $\mathbf{W}_1$ and $\mathbf{W}_2$ are both set to the same zero-thickness gap medium $\mathbf{W}_\text{g}$ for each intermediate layer. Although the gap medium's constitutive parameters are flexible, a convenient choice is $\mu_{\text{r,g}} = 1$ and $\varepsilon_{\text{r,g}} = 1+\tilde{k}_x^2+\tilde{k}_y^2$ which keeps the longitudinal wave vector component $k_{z,\text{g}}$ from being zero in a majority of cases. The only time this fails is the rare scenario when $n_\text{ref}^2\sin^2\theta = -1$. A simple fix is to use the previous constitutive parameters, and only when $n_\text{ref}^2\sin^2\theta = -1$ choose $\varepsilon_{\text{r,g}} = 4+\tilde{k}_x^2+\tilde{k}_y^2$, for example. This guarantees $\tilde{k}_{z,\text{g}} \neq 0$ regardless of incidence angle θ. With the former material choice, the gap medium eigenvector matrix is

$$\mathbf{W}_\text{g} = \frac{1}{1+\tilde{k}_x^2+\tilde{k}_y^2} \begin{bmatrix} \tilde{k}_x\tilde{k}_y & 1+\tilde{k}_y^2 & -\tilde{k}_x\tilde{k}_y & -\left(1+\tilde{k}_y^2\right) \\ -\left(1+\tilde{k}_x^2\right) & -\tilde{k}_x\tilde{k}_y & 1+\tilde{k}_x^2 & \tilde{k}_x\tilde{k}_y \\ 1+\tilde{k}_x^2+\tilde{k}_y^2 & 0 & 1+\tilde{k}_x^2+\tilde{k}_y^2 & 0 \\ 0 & 1+\tilde{k}_x^2+\tilde{k}_y^2 & 0 & 1+\tilde{k}_x^2+\tilde{k}_y^2 \end{bmatrix}. \quad (26)$$

These choices of gap medium avoid possible singularities that can arise while calculating scattering matrices as the algorithm iterates through the layers. Continuing to follow the scattering matrix approach in Ref. [4], the reflection and transmission region scattering matrices are calculated from Eqs. (23)–(25) by setting $L_i = 0$, $\mathbf{W}_i = \mathbf{W}_2 = \mathbf{W}_\text{g}$, and $\mathbf{W}_1 = \mathbf{W}_\text{ref}$ or $L_i = 0$, $\mathbf{W}_i = \mathbf{W}_1 = \mathbf{W}_\text{g}$, and $\mathbf{W}_2 = \mathbf{W}_\text{trn}$, respectively. Once the scattering matrices for the external regions and all N layers of the device are known, the global scattering matrix is calculated according to

$$\mathbf{S}^{(\text{global})} = \mathbf{S}^{(\text{ref})} \otimes \underbrace{\mathbf{S}^{(1)} \otimes \mathbf{S}^{(2)} \otimes \ldots \otimes \mathbf{S}^{(N)}}_{\mathbf{S}^{(\text{device})}} \otimes \mathbf{S}^{(\text{trn})}, \quad (27)$$

with the Redheffer star product [31] between two adjacent scattering matrices defined in general as

$$\begin{pmatrix} \mathbf{S}_{11}^{(\mathrm{AB})} & \mathbf{S}_{12}^{(\mathrm{AB})} \\ \mathbf{S}_{21}^{(\mathrm{AB})} & \mathbf{S}_{22}^{(\mathrm{AB})} \end{pmatrix} = \begin{pmatrix} \mathbf{S}_{11}^{(\mathrm{A})} & \mathbf{S}_{12}^{(\mathrm{A})} \\ \mathbf{S}_{21}^{(\mathrm{A})} & \mathbf{S}_{22}^{(\mathrm{A})} \end{pmatrix} \otimes \begin{pmatrix} \mathbf{S}_{11}^{(\mathrm{B})} & \mathbf{S}_{12}^{(\mathrm{B})} \\ \mathbf{S}_{21}^{(\mathrm{B})} & \mathbf{S}_{22}^{(\mathrm{B})} \end{pmatrix}, \quad (28)$$

$$\mathbf{S}_{11}^{(\mathrm{AB})} = \mathbf{S}_{11}^{(\mathrm{A})} + \mathbf{S}_{12}^{(\mathrm{A})} \left[\mathbf{I} - \mathbf{S}_{11}^{(\mathrm{B})}\mathbf{S}_{22}^{(\mathrm{A})}\right]^{-1} \mathbf{S}_{11}^{(\mathrm{B})}\mathbf{S}_{21}^{(\mathrm{A})},$$

$$\mathbf{S}_{12}^{(\mathrm{AB})} = \mathbf{S}_{12}^{(\mathrm{A})} \left[\mathbf{I} - \mathbf{S}_{11}^{(\mathrm{B})}\mathbf{S}_{22}^{(\mathrm{A})}\right]^{-1} \mathbf{S}_{12}^{(\mathrm{B})},$$

$$\mathbf{S}_{21}^{(\mathrm{AB})} = \mathbf{S}_{21}^{(\mathrm{B})} \left[\mathbf{I} - \mathbf{S}_{22}^{(\mathrm{A})}\mathbf{S}_{11}^{(\mathrm{B})}\right]^{-1} \mathbf{S}_{21}^{(\mathrm{A})},$$

$$\mathbf{S}_{22}^{(\mathrm{AB})} = \mathbf{S}_{22}^{(\mathrm{B})} + \mathbf{S}_{21}^{(\mathrm{B})} \left[\mathbf{I} - \mathbf{S}_{22}^{(\mathrm{A})}\mathbf{S}_{11}^{(\mathrm{B})}\right]^{-1} \mathbf{S}_{22}^{(\mathrm{A})}\mathbf{S}_{12}^{(\mathrm{B})}. \quad (29)$$

2.3. External Fields

The electric polarization vector of the source is defined as

$$\vec{P} = p_{\mathrm{TE}}\hat{a}_{\mathrm{TE}} + p_{\mathrm{TM}}\hat{a}_{\mathrm{TM}}, \quad (30)$$

where p_{TE} and p_{TM} can be any pair of complex numbers that describe the polarization state, normalized such that $|\vec{P}| = 1$ for numerical stability. The unit vectors $\hat{a}_{\mathrm{TE}}$ and $\hat{a}_{\mathrm{TM}}$ are related to the normalized incident wavevector $\vec{k}$ via

$$\hat{a}_{\mathrm{TE}} = -\sin\phi\hat{a}_x + \cos\phi\hat{a}_y, \quad (31)$$

$$\hat{a}_{\mathrm{TM}} = \frac{\vec{k} \times \hat{a}_{\mathrm{TE}}}{\left|\vec{k} \times \hat{a}_{\mathrm{TE}}\right|}, \quad (32)$$

which is only valid for interfaces in the xy plane. The mode coefficients of the incident wave $\mathbf{c}_{\mathrm{inc}}$ are calculated from the polarization vector $\vec{P}$ via

$$\mathbf{c}_{\mathrm{inc}} = \left(\mathbf{W}_{E,\mathrm{ref}}^{+}\right)^{-1} \begin{bmatrix} P_x \\ P_y \end{bmatrix}, \quad (33)$$

allowing the reflected $\mathbf{c}_{\mathrm{ref}}$ and transmitted $\mathbf{c}_{\mathrm{trn}}$ mode coefficients to be calculated as

$$\begin{bmatrix} \mathbf{c}_{\mathrm{ref}} \\ \mathbf{c}_{\mathrm{trn}} \end{bmatrix} = \begin{bmatrix} \mathbf{S}_{11}^{(\mathrm{global})} & \mathbf{S}_{12}^{(\mathrm{global})} \\ \mathbf{S}_{21}^{(\mathrm{global})} & \mathbf{S}_{22}^{(\mathrm{global})} \end{bmatrix} \begin{bmatrix} \mathbf{c}_{\mathrm{inc}} \\ \mathbf{0} \end{bmatrix}. \quad (34)$$

From these mode coefficients, the complex amplitudes of the tangential field components within the external regions are

$$\psi_{\mathrm{inc}} = \begin{bmatrix} \mathbf{W}_{E,\mathrm{ref}}^{+} \\ \mathbf{W}_{H,\mathrm{ref}}^{+} \end{bmatrix} \mathbf{c}_{\mathrm{inc}}, \quad \psi_{\mathrm{ref}} = \begin{bmatrix} \mathbf{W}_{E,\mathrm{ref}}^{-} \\ \mathbf{W}_{H,\mathrm{ref}}^{-} \end{bmatrix} \mathbf{c}_{\mathrm{ref}},$$

$$\psi_{\mathrm{trn}} = \begin{bmatrix} \mathbf{W}_{E,\mathrm{trn}}^{+} \\ \mathbf{W}_{H,\mathrm{trn}}^{+} \end{bmatrix} \mathbf{c}_{\mathrm{trn}}. \quad (35)$$

2.4. Reflection and Transmission

For conventional media, the overall fractions of power reflected R and transmitted T are

$$R = \left|\mathrm{Re}\left(\frac{\wp_{z,\mathrm{ref}}}{\wp_{z,\mathrm{inc}}}\right)\right|, \quad (36)$$

$$T = \left|\mathrm{Re}\left(\frac{\wp_{z,\mathrm{trn}}}{\wp_{z,\mathrm{inc}}}\right)\right|, \quad (37)$$

where $\vec{\wp} = \vec{E} \times \vec{H}^{*} / (2\eta_0)$ is the time-averaged Poynting vector and is calculated using the incident, reflected, or transmitted fields from Eq. (35). The absolute values in Eqs. (36) and (37) are included to address sign differences that arise when forward and backward propagating Poynting vectors are compared. These formulas are valid for most cases, including some exotic negative index external regions. However, some cases still fail, and the following discussion explains how to mitigate this.

Resolving the sign of refractive index for all cases of complex constitutive parameters remains an unsolved problem [32–34]. This sign ambiguity originates from solving $n_{\mathrm{ref}}^2 = \mu_{\mathrm{r,ref}}\varepsilon_{\mathrm{r,ref}}$ for the refractive index, which has two possible roots. Eq. (3) always assumes the positive root for simplicity. The consequence of using Eqs. (36) and (37) with the wrong root of n_{ref} results in power conservation violations, where $R + T \gg 1$, even in media without gain. This issue is resolved in either of the two following ways. First, by rerunning the simulation with $n_{\mathrm{ref}} = -\sqrt{\mu_{\mathrm{r,ref}}\varepsilon_{\mathrm{r,ref}}}$ in Eq. (3), calculate R and T via Eqs. (36) and (37). Alternatively, without rerunning the simulation, compute R and T via

$$R = \left|\mathrm{Re}\left(\frac{\wp_{z,\mathrm{inc}}}{\wp_{z,\mathrm{ref}}}\right)\right|, \quad (38)$$

$$T = \left|\mathrm{Re}\left(\frac{\wp_{z,\mathrm{trn}}}{\wp_{z,\mathrm{ref}}}\right)\right|, \quad (39)$$

which swaps the roles of the incident and reflected fields. The two methods are equivalent and yield results consistent with the Fresnel equations [2]. However, the latter approach is preferred since it avoids additional computational effort. The combination of Eqs. (36) and (37) with Eqs. (38) and (39) provides an effective method to circumvent refractive index sign ambiguities while maintaining accurate calculations of R and T.

When the real part of refractive index in the reflection region is zero $\mathrm{Re}\,[n_{\mathrm{ref}}] = 0$ and the device is composed of one or more layers, Eqs. (36)–(39) will also violate conservation to produce $R+T \gg 1$, even in media without gain. This scenario corresponds to a purely decaying plane-wave source that does not transport power to the layers. Since there cannot be power transfer in the longitudinal direction, it renders the concept of reflected and transmitted power physically meaningless in this case. Therefore, these cases should be avoided entirely.

3. IMPLEMENTATION

BTMM algorithm is summarized in the block diagram in Figure 2. The green blocks in the first column are considered the

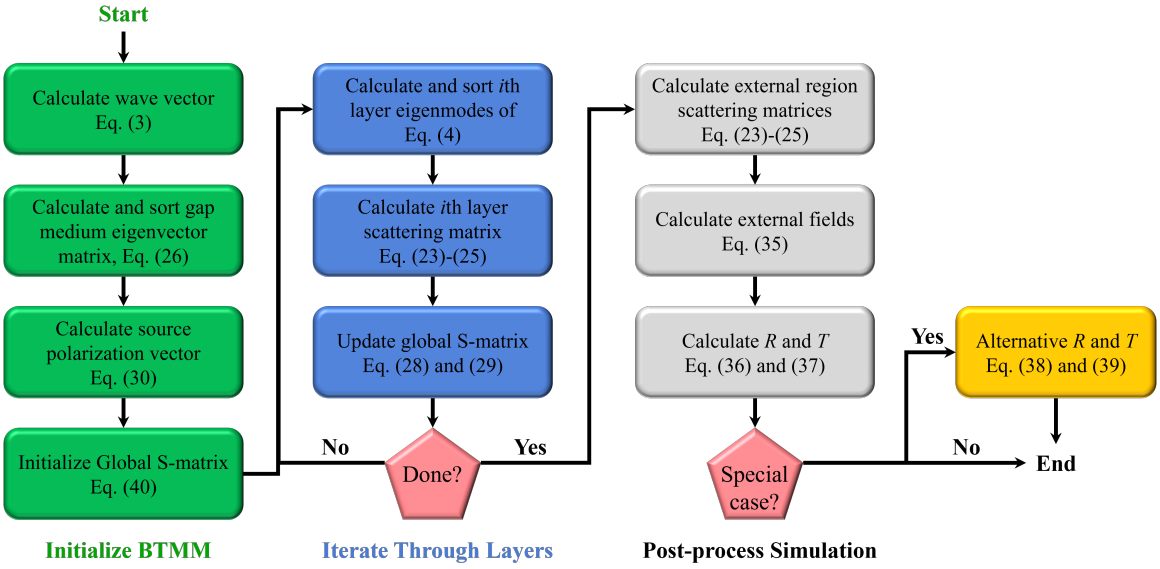

FIGURE 2. Block diagram of the BTMM algorithm.

initialization stage of the algorithm. In this stage, key parameters including the wave vector, gap medium eigenvector matrix, source fields, and global scattering matrix are initialized. The global scattering matrix is initialized to

$$\mathbf{S}_{11}^{(\text{global})} = \mathbf{S}_{22}^{(\text{global})} = \mathbf{0} \quad \text{and} \quad \mathbf{S}_{12}^{(\text{global})} = \mathbf{S}_{21}^{(\text{global})} = \mathbf{I}, \quad (40)$$

which ensures that when there are no intermediate layers, an incident wave is fully transmitted without any phase change. This is particularly useful when simulating single interface scattering between the reflection and transmission regions. Next, the algorithm processes each layer, if any, corresponding to the blue blocks in the second column. In this step, the eigenmodes for each layer are calculated and sorted. A scattering matrix for the layer is constructed and used to update the global scattering matrix. Next, the grey blocks in the third column represent the steps where the interactions with the external regions are incorporated into the global scattering matrix. This provides an easy method of calculating the external fields and determining the reflection and transmission from the device. If $R+T \gg 1$, the alternative set of reflection and transmission formulas are used.

4. BENCHMARKING

BTMM algorithm was first benchmarked against single-interface scattering examples from Ref. [2], an anisotropic device [35], and an isotropic device with bi-isotropic effective properties [11]. Then, the following two examples were selected to showcase the robustness of the BTMM algorithm and provide readers with ones to benchmark their own implementations.

The first example is of a practical yet limited bianisotropic device as simulated by the proposed BTMM algorithm. For the sake of brevity, the readers are directed to Ref. [22] for the specifics of the material properties and layer thicknesses used, as they are quite extensive. Although it should be noted that Mackay and Lakhtakia's formulation assumes the positive sign convention, the material properties must first be conjugated to fit the model of this paper. The device consists of three layers. The first is a biaxial bianisotropic layer, the second a uniaxial dielectric, and the final a Faraday chiral medium. This device is simulated for $\theta \in [0°, 90°)$ and $\phi \in [0°, 180°]$ with a source wavelength of $\lambda_0 = 560\,\text{nm}$. The absorption of this device is shown in Figure 3 for (a) TE and (b) TM polarized light, which agrees nicely with Ref. [22].

The next example device has a vacuum reflection region while the transmission region is $\varepsilon_{\text{trn}} = 2.14 - 6.92j$ and $\mu_{\text{trn}} = 5.21 - 2.27j$. The source is defined by the free-space wavelength $\lambda_0 = 1\,\text{mm}$, elevation and azimuthal angles of incidence $\theta = 29°$ and $\phi = 79°$, and a polarization state described by $p_{\text{TE}} = 0.43 - 0.39j$ and $p_{\text{TM}} = 1.00 + 0.17j$. The device consists of two nonreciprocal biaxial bianisotropic layers, with thicknesses $L_1 = L_2 = \lambda_0/16$. The tensors are rotated such that they become full and are given by

$$[\varepsilon_{\text{r},1}] = \begin{bmatrix} 3.0-4.3j & 0.3-0.3j & -1.7+0.3j \\ 0.3-0.3j & 2.1-4.9j & -0.5-0.2j \\ -1.7+0.3j & -0.5-0.2j & 4.9-4.8j \end{bmatrix}$$

$$[\xi_{\text{r},1}] = \begin{bmatrix} 3.2-4.6j & -0.2+0.5j & -0.5-0.3j \\ -0.2+0.5j & 2.2-3.3j & -0.4+0.4j \\ -0.5-0.3j & -0.4+0.4j & 3.6-4.1j \end{bmatrix}$$

$$[\zeta_{\text{r},1}] = \begin{bmatrix} 3.2-4.6j & -0.2+0.5j & -0.5-0.3j \\ -0.2+0.5j & 2.2-3.3j & -0.4+0.4j \\ -0.5-0.3j & -0.4+0.4j & 3.6-4.1j \end{bmatrix}$$

$$[\mu_{\text{r},1}] = \begin{bmatrix} 2.9-5.4j & -0.5+0.4j & -0.2-0.8j \\ -0.5+0.4j & 1.3-5.1j & -0.6 \\ -0.2-0.8j & -0.6 & 2.8-4.4j \end{bmatrix}, \quad (41)$$

$$[\varepsilon_{\text{r},2}] = \begin{bmatrix} 8.2-5.8j & 0.3+0.9j & -0.1+0.2j \\ 0.3+0.9j & 8.7-4.9j & -0.3-1.3j \\ -0.1+0.2j & -0.3-1.3j & 8.1-7.2j \end{bmatrix}$$

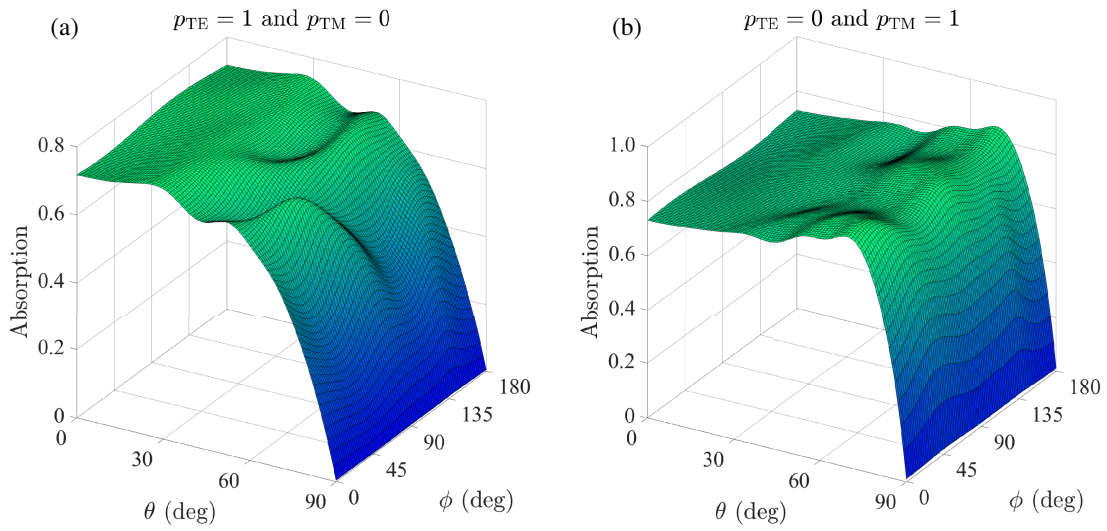

FIGURE 3. Absorption of the bianisotropic device from Ref. [22] for (a) TE and (b) TM polarized light.

$$[\xi_{\mathrm{r},2}] = \begin{bmatrix} 9.0 - 2.5j & -1.3 + 0.2j & 1.3 + 1.1j \\ -1.3 + 0.2j & 5.7 - 3.5j & 0.2 - 1.3j \\ 1.3 + 1.1j & 0.2 - 1.3j & 7.3 - 5.0j \end{bmatrix}$$

$$[\zeta_{\mathrm{r},2}] = \begin{bmatrix} 9.0 - 2.5j & -1.3 + 0.2j & 1.3 + 1.1j \\ -1.3 + 0.2j & 5.7 - 3.5j & 0.2 - 1.3j \\ 1.3 + 1.1j & 0.2 - 1.3j & 7.3 - 5.0j \end{bmatrix}$$

$$[\mu_{\mathrm{r},2}] = \begin{bmatrix} 4.8 - 8.1j & 2.3 + 0.1j & -0.3 + 0.2j \\ 2.3 + 0.1j & 8.0 - 8.2j & -2.4 - 0.4j \\ -0.3 + 0.2j & -2.4 - 0.4j & 3.2 - 8.7j \end{bmatrix}. \quad (42)$$

Simulating this device with the BTMM algorithm gives $R \approx 23.40\%$, $T \approx 2.83\%$, and overall absorption of $A = 1 - R - T \approx 73.77\%$ amongst the layers. This simulation was validated in two ways. First, the loss terms for both layers were set to zero, and conservation of power was confirmed. Second, the same device was simulated with completely different numerical approaches, an FDFD algorithm [15, 16] modified to simulate bianisotropic physics and a FEM solver (MIRaGE), which all obtained the same result.

To demonstrate the computational efficiency of the BTMM algorithm, the average run time and peak memory requirements for the previous two benchmarking examples with a fixed source are compared to those of BFDFD and BFEM in Table 1. It is important to note that direct comparisons between these methods are challenging since they are based on entirely different numerical techniques. Especially since BFDFD and BFEM require spatial discretization, convergence studies, direct solutions of large linear systems, and several other considerations are not applicable to BTMM. However, BFDFD can be loosely compared to BTMM by using one Yee cell in the xy plane with periodic boundary conditions and as many cells in the z dimension until convergence is reached. Likewise, BFEM used two transverse grid points in the xy plane with periodic boundary conditions. With respect to solving one-dimensional problems, BTMM is vastly superior to these alternatives both in time and memory requirements, often by several orders of magnitude. The BFEM approach, while the most flexible for non-planar geometries, is accompanied by significantly higher computational costs due to the 3D tetrahedral meshing of a 1D problem and reliance on a direct solver. Last, the BFDFD algorithm strikes a balance between BTMM and BFEM in terms of implementation ease and more efficient discretization over BFEM. This offers reasonable accuracy for its simplicity while not requiring specialized meshing software. All simulations converged and

TABLE 1. Average run time and peak memory for the BTMM, BFDFD, and BFEM algorithms.

Example No.	BTMM		BFDFD			BFEM		
	Avg. Time	Peak Memory	Avg. Time	Peak Memory	No. of Cells	Avg. Time	Peak Memory	No. of Elements
1	1.45 ms	16 KB	188.3 ms	2,264 KB	1224	2.28 s	130,948 KB	7940
2	1.33 ms	24 KB	26.6 ms	36 KB	320	234 ms	19,168 KB	1067

were executed on a machine with an Intel Core i7-10700k CPU @ 3.8 GHz and 32 GB of RAM.

5. CONCLUSION

This paper presented a generalization of TMM with improved scattering matrices capable of simulating devices with full nine-element material tensors for the layers and any combination of signs for the real and imaginary parts of the isotropic external regions. A detailed formulation and implementation of the algorithm was covered. Last, two bianisotropic examples were given for readers to benchmark their own implementations.

The primary purpose of formulating and implementing this algorithm was to provide the authors and other researchers with an accurate and stable numerical method for simulating reciprocal or nonreciprocal, active or passive bianisotropic layers with complex-valued external regions. Devices of this nature are of particular interest in the field of bianisotropic metamaterial research, and having an efficient simulation tool to characterize them is of vital importance. The algorithm handles the bianisotropic tensors separately and does not assume any symmetries, as is common with other bianisotropic TMM formulations found in the literature. The only known potential failure points of the algorithm are the numerical singularity when $\Omega_0 = 0$ or when $\mathrm{Re}\,[n_{\mathrm{ref}}] = 0$ with one or more layers. Future work on this algorithm can include addressing the $\mathrm{Re}\,[n_{\mathrm{ref}}] = 0$ failure point (if fixable), nonlinear material properties, and/or allowing for bianisotropic external regions.

ACKNOWLEDGEMENT

This material is based upon work supported by, or in part by, the U. S. Army Research Laboratory and the U. S. Army Research Office under Grant No. W911NF2020194.

REFERENCES

[1] Billard, J., "Contribution a l'etude de la propagation des ondes electromagnetiques planes dans certains milieux materiels (2ème these)," Université de Paris, Paris, France, 1966.

[2] Macleod, H. A., *Thin-Film Optical Filters*, CRC Press, 2010.

[3] Hodgkinson, I. J. and Q. H. Wu, *Birefringent Thin Films and Polarizing Elements*, World Scientific, 1997.

[4] Rumpf, R. C., "Improved formulation of scattering matrices for semi-analytical methods that is consistent with convention," *Progress In Electromagnetics Research B*, Vol. 35, 241–261, 2011.

[5] Castillo-Tapia, P., K. V. Gassen, Q. Chen, F. Mesa, Z. Sipus, and O. Quevedo-Teruel, "Dispersion analysis of twist-symmetric dielectric waveguides," *Photonics*, Vol. 8, No. 6, 206, Jun. 2021.

[6] Alex-Amor, A., A. Palomares-Caballero, F. Mesa, O. Quevedo-Teruel, and P. Padilla, "Dispersion analysis of periodic structures in anisotropic media: Application to liquid crystals," *IEEE Transactions on Antennas and Propagation*, Vol. 70, No. 4, 2811–2821, Apr. 2022.

[7] Hong, J., W. Huang, and T. Makino, "On the transfer matrix method for distributed-feedback waveguide devices," *Journal of Lightwave Technology*, Vol. 10, No. 12, 1860–1868, Dec. 1992.

[8] Li, Z.-Y. and L.-L. Lin, "Photonic band structures solved by a plane-wave-based transfer-matrix method," *Physical Review E*, Vol. 67, No. 4, 046607, Apr. 2003.

[9] Kron, G., "Equivalent circuit of the field equations of Maxwell-I," *Proceedings of the IRE*, Vol. 32, No. 5, 289–299, May 1944.

[10] Smith, D. R. and J. B. Pendry, "Homogenization of metamaterials by field averaging (Invited Paper)," *Journal of the Optical Society of America B*, Vol. 23, No. 3, 391–403, Mar. 2006.

[11] Kriegler, C. E., M. S. Rill, S. Linden, and M. Wegener, "Bianisotropic photonic metamaterials," *IEEE Journal of Selected Topics in Quantum Electronics*, Vol. 16, No. 2, 367–375, 2010.

[12] Rumpf, R. C. and E. G. Johnson, "Modeling fabrication to accurately place GMR resonances," *Optics Express*, Vol. 15, No. 6, 3452–3464, Mar. 2007.

[13] Moharam, M. G., E. B. Grann, D. A. Pommet, and T. K. Gaylord, "Formulation for stable and efficient implementation of the rigorous coupled-wave analysis of binary gratings," *Journal of the Optical Society of America A*, Vol. 12, No. 5, 1068–1076, May 1995.

[14] David, A., H. Benisty, and C. Weisbuch, "Fast factorization rule and plane-wave expansion method for two-dimensional photonic crystals with arbitrary hole-shape," *Physical Review B*, Vol. 73, No. 7, 075107, Feb. 2006.

[15] Rumpf, R. C., C. R. Garcia, E. A. Berry, and J. H. Barton, "Finite-difference frequency-domain algorithm for modeling electromagnetic scattering from general anisotropic objects," *Progress In Electromagnetics Research B*, Vol. 61, 55–67, 2014.

[16] Rumpf, R. C., *Electromagnetic and Photonic Simulation for the Beginner: Finite-Difference Frequency-Domain in MATLAB®*, Artech House, 2022.

[17] Pehrabad, S. N., M. Y. Wang, and B. Liu, "Propagation characteristics of layered bianisotropic chiral media based on transfer matrix method," in *2024 Photonics & Electromagnetics Research Symposium (PIERS)*, 1–6, Chengdu, China, Apr. 2024.

[18] Ning, J. and E. L. Tan, "Hybrid matrix method for stable analysis of electromagnetic waves in stratified bianisotropic media," *IEEE Microwave and Wireless Components Letters*, Vol. 18, No. 10, 653–655, Oct. 2008.

[19] Hajesmaeili, H. N., M. Zamani, and M. H. Zandi, "Bi-gyrotropic single-negative magnetic materials in the presence of longitudinal magnetization: A transfer matrix approach," *Photonics and Nanostructures — Fundamentals and Applications*, Vol. 24, 69–75, May 2017.

[20] Ren, X., S. Zhang, F. Yong, and M. Wang, "Transfer matrix method study on interaction of electromagnetic waves with stratified biaxial bianisotropic chiral media," in *2021 13th International Symposium on Antennas, Propagation and EM Theory (ISAPE)*, 1–3, Zhuhai, China, Dec. 2021.

[21] Yin, W. Y., G. H. Nan, and I. Wolff, "The combined effects of chiral operation in multilayered bianisotropic substrates," *Progress In Electromagnetics Research*, Vol. 20, 153–178, 1998.

[22] Mackay, T. G. and A. Lakhtakia, *The Transfer-Matrix Method in Electromagnetics and Optics*, Springer Nature, 2022.

[23] Yang, X., L. Lei, and J. Hu, "The hybrid embedded domain decomposition method for scattering by bi-anisotropic objects," in *2021 IEEE International Symposium on Antennas and Propagation and USNC-URSI Radio Science Meeting (APS/URSI)*, 1093–1094, Singapore, Dec. 2021.

[24] Zhang, Y., X. Wei, and E. Li, "Electromagnetic scattering from three-dimensional bianisotropic objects using hybrid finite element-boundary integral method," *Journal of Electromagnetic Waves and Applications*, Vol. 18, No. 11, 1549–1563, Jan. 2004.

[25] Akyurtlu, A. and D. H. Werner, "BI-FDTD: A novel finite-difference time-domain formulation for modeling wave propagation in bi-isotropic media," *IEEE Transactions on Antennas*

and Propagation, Vol. 52, No. 2, 416–425, Feb. 2004.

[26] Guo, Q., W. Gao, J. Chen, Y. Liu, and S. Zhang, "Line degeneracy and strong spin-orbit coupling of light with bulk bianisotropic metamaterials," *Physical Review Letters*, Vol. 115, No. 6, 067402, Aug. 2015.

[27] Reyes-Avendaño, J. A., M. P. Sampedro, E. Juárez-Ruiz, and F. Pérez-Rodríguez, "Bianisotropic metamaterials based on twisted asymmetric crosses," *Journal of Optics*, Vol. 16, No. 6, 065102, Jun. 2014.

[28] Li, Z., K. Aydin, and E. Ozbay, "Determination of the effective constitutive parameters of bianisotropic metamaterials from reflection and transmission coefficients," *Physical Review E*, Vol. 79, No. 2, 026610, Feb. 2009.

[29] Mackay, T. G. and A. Lakhtakia, *Electromagnetic Anisotropy and Bianisotropy: A Field Guide*, World Scientific, 2010.

[30] Wood, R. W., "XLII. On a remarkable case of uneven distribution of light in a diffraction grating spectrum," *The London, Edinburgh, and Dublin Philosophical Magazine and Journal of Science*, Vol. 4, No. 21, 396–402, 1902.

[31] Redheffer, R., "Inequalities for a matrix riccati equation," *Journal of Mathematics and Mechanics*, Vol. 8, No. 3, 349–367, 1959.

[32] Sheldon, B., J. S. Haggerty, and A. G. Emslie, "Exact computation of the reflectance of a surface layer of arbitrary refractive-index profile and an approximate solution of the inverse problem," *Journal of the Optical Society of America*, Vol. 72, No. 8, 1049–1055, Aug. 1982.

[33] Afanas'ev, S. A., D. G. Sannikov, and D. I. Sementsov, "The refractive index sign chosen for amplifying and lossy metamaterials," *Journal of Communications Technology and Electronics*, Vol. 58, 1–11, Jan. 2013.

[34] Wei, J. and M. Xiao, "Electric and magnetic losses and gains in determining the sign of refractive index," *Optics Communications*, Vol. 270, No. 2, 455–464, Feb. 2007.

[35] Shenk, J. O., R. P. Ingel, Y. Cao, and M. A. Fiddy, "Anisotropic periodic structure exhibiting gigantic field enhancements," in *Micro-Optics 2008*, Vol. 6992, 209–217, Strasbourg, France, 2008.